Hall Thruster with an External Acceleration Zone

IEPC-2005-196

Presented at the 29th International Electric Propulsion Conference, Princeton University, October 31 – November 4, 2005

Nicolas Gascon*, Ronald L. Corey† and Mark A. Cappelli‡
Stanford University, Stanford, CA, 94305, USA

and

William A. Hargus, Jr§
Air Force Research Laboratory, Edwards AFB, 93524, USA

This work presents a study of the external acceleration operating mode of a low-power linear-geometry Hall thruster. Measurements are reported of the performance and of the near exit plane ion velocity field in a high vacuum environment. Thrust and efficiency were measured at Stanford University, while ion velocities were measured in a similar vacuum environment at the Air Force Research Laboratory, using laser induced fluorescence of the excited state xenon ionic transition at 834.7 nm. Velocities were measured primarily in the near field, from the channel exit plane to a downstream distance of 3 cm. Both axial and cross-field (along the electron Hall current direction) component velocities were measured. The results presented here, combined with those of previous studies, highlight the high sensitivity of the electron mobility to discharge properties inside and outside of the channel, such as background gas density, wall material, or magnetic field strength. When operated at low background pressure, this particular linear Hall discharge creates an ion accelerating electrostatic field that is 0.5 – 2 cm downstream of the exit plane, well outside of the channel. This interesting mode of operation is attributed to the reduced electron impendence due to wall current at the terminating end of the electron drift. In this particular design, the consequence is a reduced level of performance, because of the non-ideal magnetic field configuration in the acceleration region. However, it suggests the possibility of new opportunities towards developing so-called wall-less Hall thruster, which have the promise of lower wall erosion.

I. Introduction

MODERN day operational Hall thrusters are closed electron drift magnetized discharges with an uninterrupted electron Hall current[1]. In recent years, however, we have demonstrated the feasibility of an "open-drift", linear Hall thruster[3-5]. Such a geometry is attractive for scaling down the discharge, because it does not have the practical limitations imposed by the central magnet pole piece in a coaxial design, and affords the possibility of a more favorable magnetic field configuration. Another motivation for developing this linear Hall thruster design is that it has accommodated the testing of advanced ceramic materials for future co-axial designs that are not easily machined but are available in plate form. An example of such a promising ceramic is chemical vapor deposited (CVD) polycrystalline diamond. This material appears to be a good alternative to boron nitride (BN) based ceramics that are commonly used on modern Hall thrusters, especially at lower powers, because if its higher thermal conductivity and lower thermal expansion coefficient (resulting in lower thermal and mechanical stress), lower

* Research Associate, Mechanical Engineering Department, Thermosciences Group, MC 3032.
† Research Assistant, Mechanical Engineering Department, Thermosciences Group, MC 3032.
‡ Professor, Mechanical Engineering Department, Thermosciences Group, MC 3032.
§ Research Engineer, Spacecraft Propulsion Branch, 1 Ara Rd.

erosion rate under ion bombardment (hence longer lifetime), and potentially lower secondary electron yield (higher acceleration efficiency).

In previous work[5,6], we showed that a Hall thruster can indeed operate well with CVD diamond walls, with a lower discharge current than with BN walls (all other input parameters being equal), and with a much higher resistance to sputtering under ion bombardment (at least three times higher than BN). Although we measured almost equal ion currents in the plume of the diamond-lined and the BN-lined discharges, a hint that the former is more efficient, we did not record direct thrust and performance data at that time. Also, these prior experiments were conducted in vacuum chambers that had relatively high background pressures (on the order of 0.01 Pa), and in some cases noticed that the chamber pumping mechanism (oil diffusion or cryogenic) had a measurable effect on the discharge behavior. Finally, we discovered that the diamond-lined thruster could operate in an intriguing mode, stable but pulsed, where the discharge was apparently pushed well outside of the channel.

These results prompted us to further investigate the performance and the ion acceleration of this unusual Hall thruster. In this present study, we characterize the operation of the Stanford Linear Hall Thruster (LHT) in two similar high-vacuum facilities ($< 5\times10^{-4}$ Pa) – one at Stanford University, and the other at the Air Force Research Laboratory (Edwards AFB). Measurements at Stanford include efficiency, thrust and specific impulse. At AFRL, we probe the near exit ion velocity field using excited state xenon Laser Induced Fluorescence (LIF). The results presented in this paper indicate that for this particular linear Hall thruster geometry and in a sufficiently high vacuum environment, the majority of the ion's acceleration (> 95 %) is well outside of the channel.

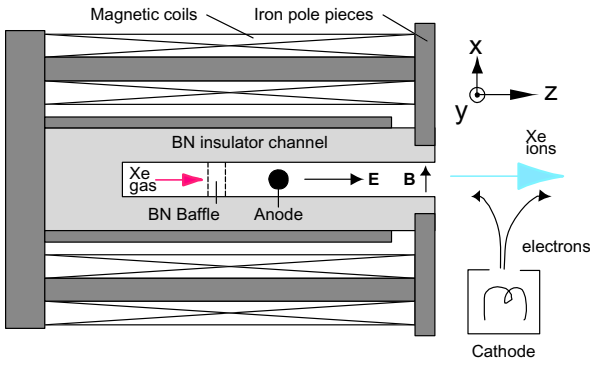

Figure 1. Stanford Linear Hall Thruster schematic.

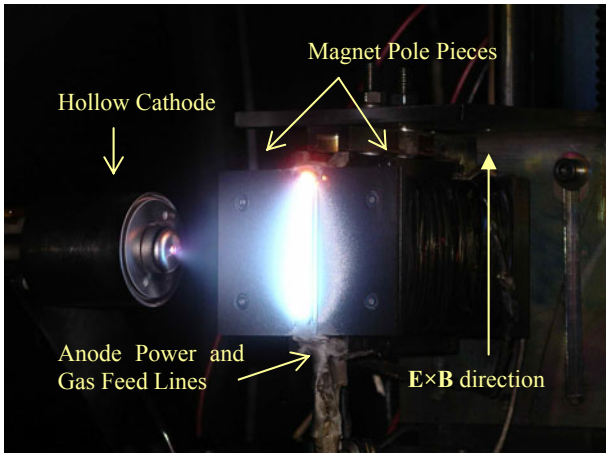

Figure 2. Stanford LHT viewed from a 45° angle, operating in chamber 6 at AFRL.

II. Experiments

A. Thruster

The details of the linear Hall thruster operated here are described in previous papers[5,6]. The discharge and the experimental set-up, along with the coordinate system used in this paper, are shown in Fig. 1. Note that the *X* direction corresponds to the radial direction in a classical (annular) Hall thruster. The *Y* direction is parallel to the ***E*×*B*** electron drift. The *Z* direction follows the ***E*** field direction, and consequently, the major axis of the ion stream. The magnetic circuit is built from cast gray iron and consists of two rectangular solenoid coils, two front pole pieces, and one back pole piece. A magnetic screen is also used to sharpen the magnetic field profile, which is maximum in strength between the pole pieces. For the nominal operating coil current of 1 A, this peak magnetic field is approximately 80 mT, and the field strength at the anode is over 10 mT. The field has excellent uniformity (<1 % variation) along the *Y* direction. The supporting channel structure is made of boron nitride, and is machined with two pockets that allow 1 mm thick rectangular plates of different wall materials to be tested. A boron nitride baffle separates a plenum from the anode, which is a simple solid tungsten rod 1.6 mm in diameter.

A commercial hollow cathode (Veeco/IonTech HCN-252) is used to neutralize the ion beam. This cathode is located 30 mm downstream of the channel exit, 45 mm from the channel in *X* and centered in *Y*. The thruster is

mounted such that the *Y* direction is vertical and the *X* and *Z* directions are horizontal. During thruster operation, the discharge chamber wall facing the ***E*×*B*** direction becomes red hot due to intense electron bombardment, as can be clearly seen in Fig. 2. The nominal input parameters include a xenon flow rate of 0.6 mg/s, an electromagnet current of 1 A, a discharge voltage of 200 V, and a cathode xenon flow rate of 0.15 mg/s. Both the BN-channel and diamond-channel thrusters proved capable of continuous operation at voltages as high as 300 V.

B. Vacuum facilities and diagnostics at Stanford University

The LHT thrust efficiency measurements were performed at Stanford University's plasma propulsion testing facility, which is a 3.25 m long nonmagnetic stainless steel vacuum chamber, 1.25 m in diameter. During nominal operation of the thruster, the pressure inside the chamber is kept to approximately 3×10^{-4} Pa (as measured using an ion gauge uncorrected for xenon) by a two-stage cryogenic pumping system (CVI, model number TM1200) cooled down by a helium refrigerator for the cryopanels and a flow of liquid nitrogen for the shroud. Separate DC power supplies are used for the discharge, cathode keeper, cathode heater, and electromagnets. The thruster is electrically isolated from the supporting structure. The macroscopic thruster parameters (discharge voltage, anode current, etc.) are monitored and recorded at a 1 Hz data rate with an Agilent data logging system.

Thrust is measured using an inverted pendulum type scale, which is represented schematically in Fig. 3. The lower portion of the inverted pendulum is fixed to the vacuum chamber. The thruster is mounted upon the upper pendulum portion, which is kept horizontal by using an inclinometer for monitoring and a remotely controlled lever for adjusting the thrust stand inclination. The two pendulum portions are connected by several flexures, a restoring spring, the calibration system, the propellant feed lines and the electrical power lines. An electromagnetic damper restrains oscillations that couple into the thrust stand from the test environment. The displacement of the inverted pendulum is converted into a proportional voltage signal by a linear variable differential transformer (LVDT) made by Macro Sensors, model PR 812. The LVDT output signal is monitored and sampled at a 10 Hz rate with the Agilent data logging system, and the traces are recorded on a personal computer for further analysis. The thrust stand is water cooled to minimize the signal drift due to uneven thermal expansion of the various structure parts when the discharge is running. Calibration of the thrust stand is performed using an electric motor and pulley system. Weights are suspended from the pulley attached to the inverted pendulum. The electric motor lowers or raises several weights of known masses (within 10^{-4} relative uncertainty). The deflection of the inverted pendulum for known calibration weights yields a linear displacement versus calibration force curve. Multiple thrust measurements and calibrations in various pressure and thruster operating condition have demonstrated that the system is linear within 1% tolerance and capable of detecting horizontal forces as weak as 0.1 mN.

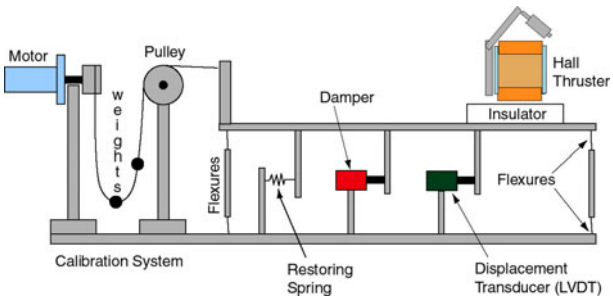

Figure 3. Stanford thrust stand schematic.

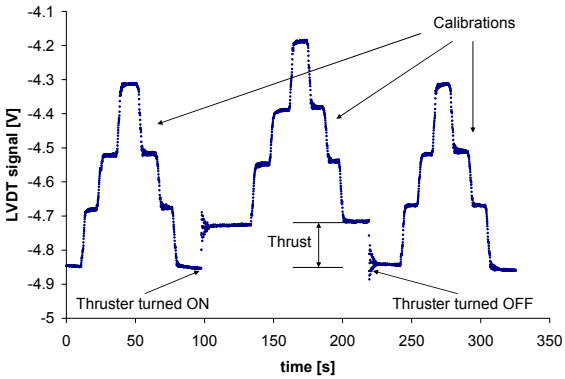

Figure 4. Sample LVDT signal trace recorded during thruster operation and thrust stand calibration.

For the thrust measurements presented hereafter, we systematically use 3 calibrations weights. The LHT is warmed up at nominal operating conditions until no noticeable drift is observed in the discharge current and in the LVDT signal, then the discharge is turned off. Figure 4 describes what happens next. The reference signal (discharge off), the thrust signal (discharge on), and then the reference signal again are recorded for at least 10 s and calibrated. The whole procedure is repeated 5 times for every operating point. It should be noted that the xenon gas is always flowing through the anode and the cathode during the whole procedure. The extra force due to the cold gas

expanding in vacuum is not taken into account in our measurements, but we verified that it amounts to only a few percents of the total thrust, at most.

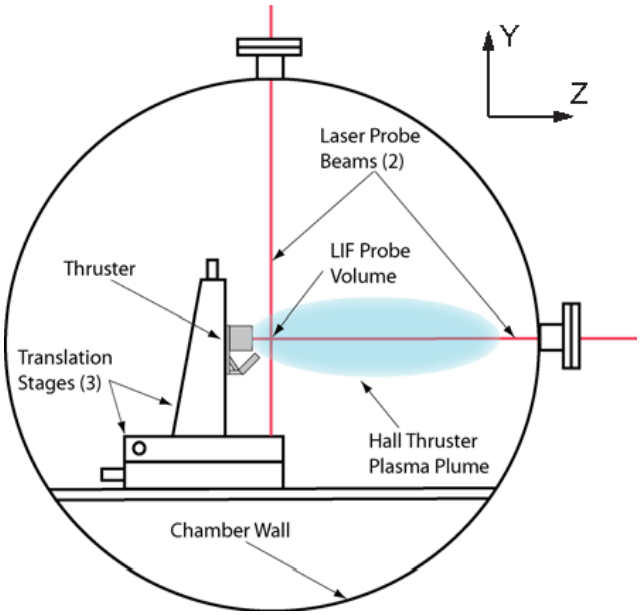

Figure 5. Side view diagram of the thruster, translation stages and laser probe beams within AFRL Chamber 6. Note that the fluorescence collection and external optics are not shown.

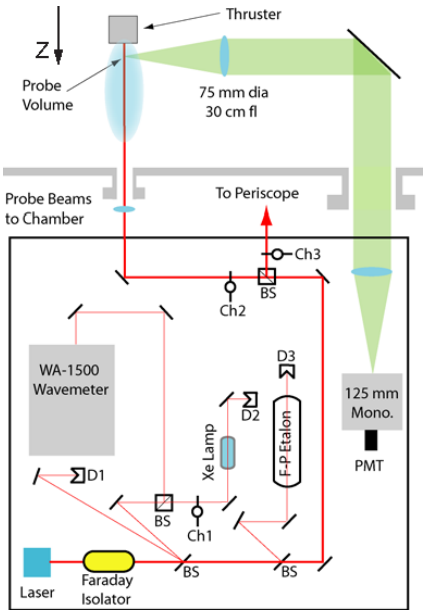

Figure 6. Top view diagram of the laser optical train and collection optics. Note that the radial probe beam periscope and focusing optics are not shown.

C. Vacuum facilities and diagnostics at AFRL

The LIF measurements were performed in Chamber 6 at the Air Force Research Laboratory's (AFRL) Electric Propulsion Laboratory at Edwards Air Force Base in California, which has vacuum characteristics similar to the facility at Stanford University. The Chamber 6 vacuum facility is made of nonmagnetic stainless steel and has a 1.8 m diameter and 3.0 m length. Chamber pressure during thruster operation is maintained to about 3×10^{-4} Pa by a cryogenic pumping system. Figure 5 shows a side-view diagram of the LHT mounted on a three-axis orthogonal computer controlled translation system inside AFRL Chamber 6.

Figure 5 also shows the two orthogonal LIF probe beams and windows through which the beams enter the chamber. Figure 6 shows a top view of the laser optical train, collection optics, and one leg of the external probe optics. The laser used is a New Focus Vortex tunable diode laser, capable of tuning approximate ±50 GHz about a center wavelength of 834.7 nm. The laser is controlled by an analog ramp signal generated by a National Instruments E-series data acquisition board. During each laser scan, the data acquisition card records the absorption and two fluorescence signals using three lock-in amplifiers, and the signal from a Fabry Perot etalon photodiode detector (D3 in Fig. 6) using a current preamplifier. Typically, the scans span 55 GHz. Each scan yields four traces of several thousand points. The traces are then stored for post processing.

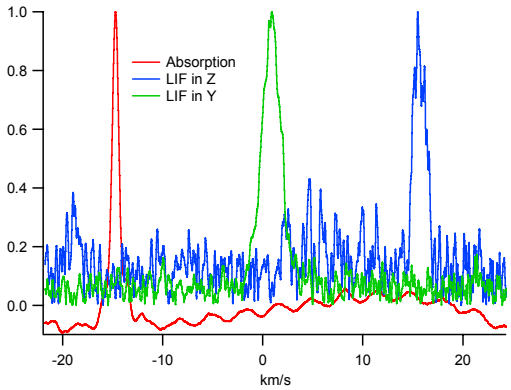

Figure 7. Sample LIF/absorption traces. All signals have been normalized. BN walls, nominal operating conditions, z = +30 mm, $x = y = 0$.

The origin of all the velocity maps is located at the thruster exit plane, centered in the *Y* and *X* direction. For the experiments presented here, the thruster was moved along the *Z* direction (i.e. along the principal direction of

the plasma), as far as 30 mm away from the exit plane. The LIF apparatus allowed measuring the ion velocity components along the Z and Y axis. Figure 7 shows an example of processed scan, with the V_z and V_y distributions, and the reference absorption signal. For this particular scan, the velocity distributions are close to Gaussians with half-widths on the order of a few km/s. The V_z distribution peaks near 16 km/s, corresponding to an ion energy of about 170 eV (as a reminder, the discharge voltage is 200 V). The V_y distribution peaks near 2 km/s in the positive ($\boldsymbol{E}_z \times \boldsymbol{B}_y$) direction, which results probably from the asymmetry caused by the electron Hall current. In other scans not shown here, the velocity distributions came out less regular than the ones presented in Fig. 7, which can be explained by several mechanisms: an ionization zone widely spread across the plasma potential drop, bulk plasma oscillations[8], or momentum and charge exchange collisions with the xenon atoms. In the LIF maps presented below, we chose to plot the most probable velocity component (peak of the velocity distribution) together with the average velocity component (i.e. the first moment of the distribution).

III. Results and discussion

Figure 8 shows the current voltage characteristics of the Stanford LHT for various combinations of wall materials (BN or diamond), anode xenon flow rate (0.9 or 0.6 mg/s) and electromagnet current (0.5 or 1.0 A). It is apparent from these curves that the LHT discharge current does not reach a plateau at high applied voltages (> 150 V) but continues to increase, unlike what is observed with most modern, co-axial Hall thrusters. This seems to indicate that in the case of the LHT, a voltage-dependent mechanisms provides an added electron current in the discharge when the ionization fraction has reached a maximum. We surmise that this additional current is a cross field electron flow created by a strong near-wall conductivity effect[9] on the channel side facing the Hall current. The nature of the wall material, boron nitride or CVD diamond, does not seem to have a significant impact on the discharge current. However, our previous studies of this particular linear Hall discharge using diamond instead of boron nitride for the channel inserts always resulted in a lower discharge current, or even a change in operating regime[5,6].

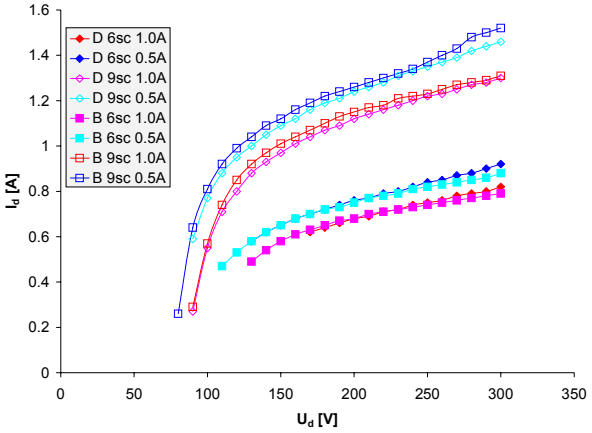

Figure 8. Current-Voltage characteristics of the Stanford LHT for various operating conditions. Squares: with BN walls. Diamonds: with CVD diamond walls. Full Markers: 0.6 mg/s anode flow rate. Empty Markers: 0.9 mgs/s anode flow rate. Blue Plots: 0.5 A electromagnet current. Red Plots: 1.0 A electromagnet current.

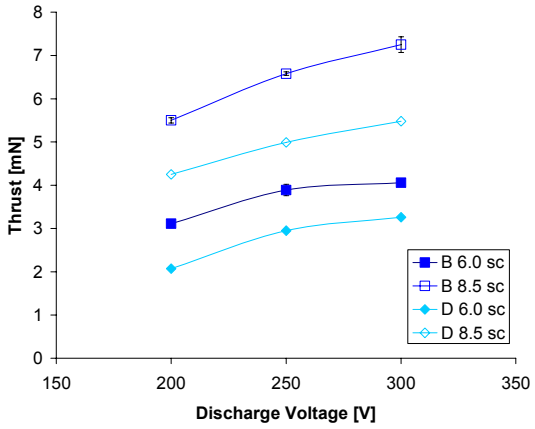

Figure 9. Thrust-Voltage characteristics of the Stanford LHT, for various operating conditions. Squares: with BN walls. Diamonds: with CVD diamond walls. Full Markers: 0.6 mg/s anode flow rate. Empty Markers: 0.85 mgs/s anode flow rate.

The performace measurement results are summarized in Table 1. An unexpected result in the comparison of performance for the case of BN and diamond walls, is that the BN lined LHT produced an overall higher thrust, despite the virtually identical I-V characteristics. A comparison of the thrust for two values of the mass flow rate, and over a limited range of discharge voltage is shown in Fig. 9. It appears as though the BN-lined walls have a 15 – 25 % higher thrust than the diamond-lined walls. This result is surprising, and the reason for this difference is not yet understood. The similar discharge current would imply that the ion current is lower in the case of the diamond-lined thruster. A lower ion current is due either to a lower ion velocity, or lower plasma density. An attempt is made to resolve this question through LIF measurements of the ion velocity, as described below.

Table 1. Performance Parameters.

Wall material	P_{back}, Pa	U_D, V	I_D, A	Input power, W	Flow rate, mg/s	Thrust, mN	I_{sp}, s	η
BN	1.90×10^{-4}	200	0.55	110	0.6	3.11	528	0.073
BN	1.90×10^{-4}	250	0.60	151	0.6	3.89	661	0.084
BN	1.90×10^{-4}	300	0.63	189	0.6	4.06	690	0.073
BN	2.30×10^{-4}	200	0.97	194	0.85	5.50	659	0.092
BN	2.30×10^{-4}	250	1.05	263	0.85	6.58	789	0.097
BN	2.30×10^{-4}	300	1.10	330	0.85	7.25	870	0.094
Diamond	1.90×10^{-4}	200	0.56	112	0.6	2.07	352	0.032
Diamond	2.50×10^{-4}	250	0.61	153	0.6	2.95	501	0.047
Diamond	2.50×10^{-4}	300	0.63	189	0.6	3.26	554	0.047
Diamond	2.50×10^{-4}	200	0.98	196	0.85	4.25	510	0.054
Diamond	2.50×10^{-4}	250	1.05	263	0.85	4.99	598	0.056
Diamond	2.50×10^{-4}	300	1.09	326	0.85	5.48	657	0.054

Figures 10 and 11 graph the axial variation in the axial component (*Z* direction) and Hall-component (*Y* direction), of the mean and peak ion velocities. A comparison between the case of a BN-lined (Fig. 10) and diamond-lined (Fig. 11) thruster reveals that when the LHT is operated in AFRL Chamber 6, the ion dynamics in the plume is mostly unaffected by the type of channel wall inserts, i.e. the BN and diamond cases are similar within experimental uncertainty. This implies that the difference in the thrust measured, if real, must be due to a difference in plasma density – a result that we must indpendently verify in a future study. Another interesting finding is that upon examination of the axial velocity profiles, it is apparent that a portion of the ion acceleration occurs outside the thruster, 5 – 20 mm away from the exit plane. This external acceleration was not expected, and to our knowledge, has not been previously seen in Hall thrusters. We believe that in our previous studies of this particular linear geometry thruster, this external acceleration mode may have been masked by the relatively high chamber pressures used in the experiments discussed in Refs. 2 – 6. At high background chamber pressure, collisions between atoms and electrons account for a high cross-magnetic field mobility, and most of the plasma potential drop occurs inside the channel. In the experiments presented here, the results suggest that the cross-field electron mobility due to the background gas *outside* the channel is lower than the one due to the drift-terminating side wall *inside* the channel.

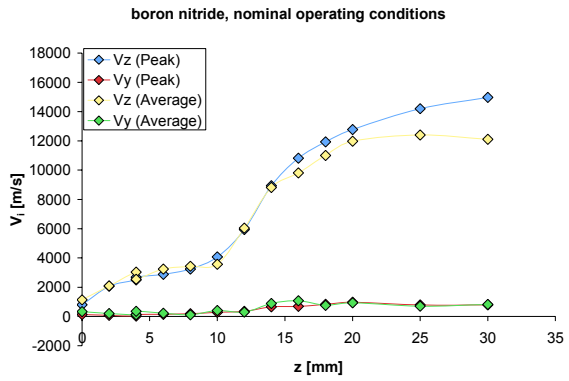

Figure 10. Velocities for BN walls, nominal case.

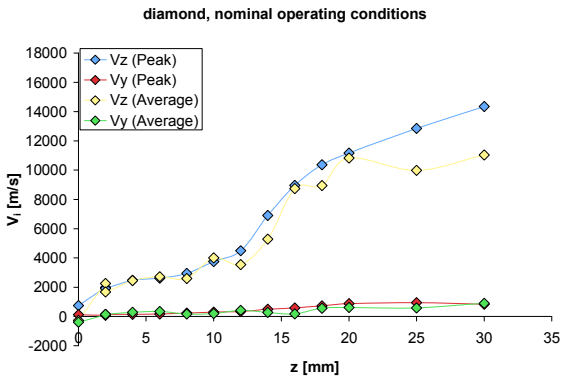

Figure 11. Velocities for diamond wall, nominal case.

The effect of background neutral gas is again illustrated in Fig. 12, where the cathode xenon flow rate is doubled (to 0.3 mg/s) compared to the nominal condition (0.15 mg/s). A doubling of the cathode flow in the vicinity of the exit of the channel would in effect increase (perhaps double) the local gas density. This condition results in a significant shift in the major acceleration region, as it is seen to move upstream by about 5 – 7 mm. In fact, in contrast with the nominal case, we see that with the higher cathode flow rate, there is almost no ion acceleration around the location of the cathode ($z = 30$ mm). Apparently, the increased density results in a weaker electrostatic field and a high electron cross-magnetic field mobility. Also evident in Fig. 12 is a greater difference between the most probable velocities and the average velocities when compared to the velocities in Fig. 10. We speculate that

this is the result of increased charge exchange collisions near the cathode skewing the ion energy distribution. An increase in the anode flow by 50 % (see Fig. 13) is seen to have almost no effect on the overall acceleration process. This is an interesting result, as it confirms the significant degree of propellant utilization common in Hall thrusters. It seems that the neutral propellant that escapes the ionization process has less of an effect on the near-field than does the high degree of unionized xenon emitted from the cathode.

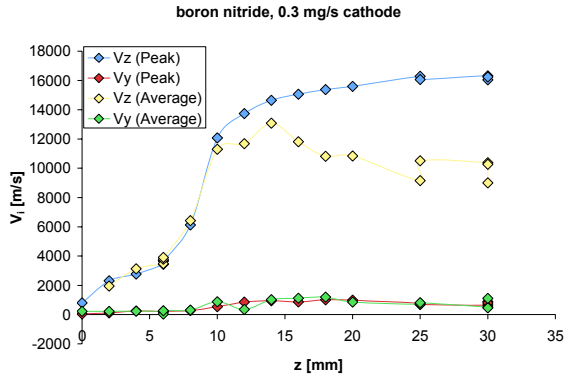

Figure 12. Velocities for BN walls LHT with increased cathode flow.

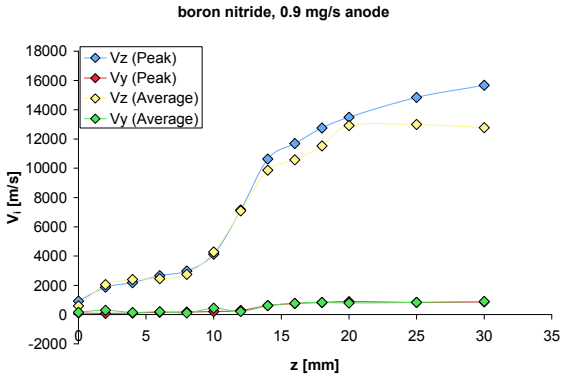

Figure 13. Velocities for BN walls LHT with increased anode flows.

Finally, the experimental results presented in Fig. 14 address the role that the magnetic field has on establishing the local plasma conductivity in the region of the acceleration zone. When the magnetic flux density is reduced by a factor two by reducing the magnetic current, the region over which the acceleration takes place is noticeably broadened. The velocity reaches the same final value, since the discharge voltage is kept constant; however, it does so over a greater distance.

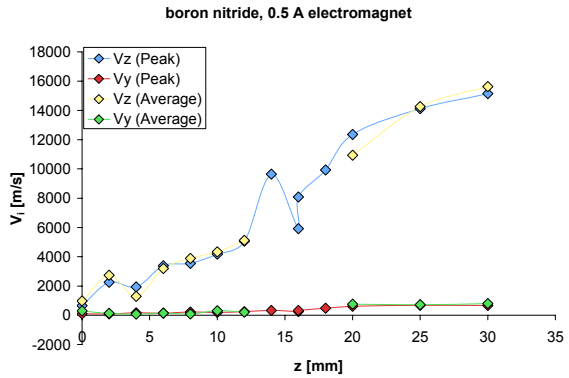

Figure 14. Velocities for BN walls LHT with reduced magnetic field.

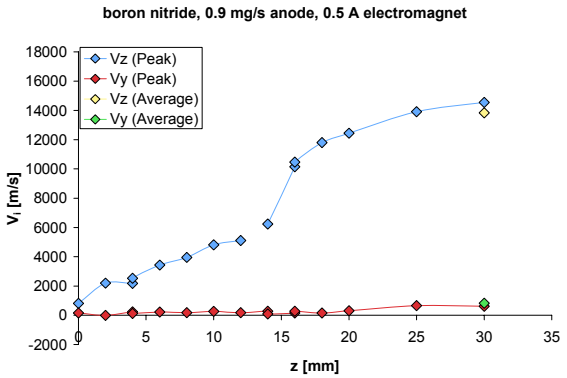

Figure 15. Velocities for BN walls LHT with increased anode flow and reduced magnetic field.

IV. Summary and Future Work

We have characterized the operation and performance of a linear-geometry Hall thruster in a high vacuum environment, and have carried out Laser Induced Fluorescence measurements of the near exit xenon ion velocity field. These results, considered together with previous studies on the same thruster, highlight the importance of the near-field environment on the electron mobility inside and outside the channel. In particular, we have found that the cathode flow rate greatly affects the acceleration process, which for this thruster, appears outside of the channel. As expected, the strength of this acceleration also depends on the magnetic field, which is another factor controlling the electron mobility. We believe that the external acceleration seen in this linear Hall thruster configuration is unique, although this is seen to take place only in test facilities with sufficiently low chamber pressure. At higher chamber

pressures, the acceleration zone moves back towards the exit plane, and at pressures similar to where it has been tested earlier, most likely into the channel. At this point, it is difficult to make broad conclusions about this phenomenon as it pertains to co-axial discharge configurations, in that the external acceleration may be a consequence of the terminated Hall current. However, an external acceleration zone and a concomitant reduction in performance may be a possible trade-off in applications requiring greatly extended thruster throughput. At present, we are examining more optimized magnetic field configurations that enhance performance of such "wall-less" Hall thrusters with external ion acceleration.

Acknowledgments

This work is funded in part by the Air Force Office of Scientific Research. The authors would like to thank J. Zimmer and J. Herlinger (*sp*^{3} Inc.) for providing the diamond plates used in this study, and C. McLean (Pratt and Whitney) for his original assistance with the configuration of the thrust stand.

References

[1]Zhurin V. V., and Kaufman H. R., "Physics of Closed Drift Thrusters" *Plasma Sources Sci. Technology* **8**, pp. R1-R20, 1999.

[2]Hargus W. A., Jr, and Cappelli M. A., "Development of a Linear Hall Thruster", *34th Joint Propulsion Conference, Cleveland, OH*. American Institute of Aeronautics and Astronautics, Washington, DC, 1998. AIAA-98-3336.

[3]Schmidt D. P., Meezan N.B., Hargus W.A., Jr., and Cappelli M.A., "A Low-Power, Linear-Geometry Hall Plasma Source with an Open Electron-Drift," *Plasma Sources Science and Technology* 9, pp. 68-76, 2000.

[4]Cappelli M.A., Walker Q.E., Meezan N.B., and Hargus W.A., Jr., "Performance of a Linear Hall Discharge with an Open Electron Drift", *37th Joint Propulsion Conference, Salt Lake City, UT*, American Institute of Aeronautics and Astronautics, 2001. AIAA-2001-3503.

[5]Meezan N. B., Gascon N., and Cappelli M. A., "Linear Geometry Hall Thruster with Boron Nitride and Diamond Walls", 27th International Electric Propulsion Conference, Pasadena, CA. Electric Rocket Propulsion Society, 2001. IEPC-01-39.

[6]Gascon, N., Thomas, W. A., Hermann, W. A., and Cappelli M. A., "Operating regimes of a linear SPT with low secondary electron-induced wall conductivity", *39th AIAA/ASEE/ASME Joint Propulsion Conference, Huntsville, Alabama*. American Institute of Aeronautics and Astronautics, Washington, DC, 2003. AIAA-2003-5156.

[7]Hargus W. A., Jr, and Charles C., "Near Exit Plane Velocity Field of a 200 W Hall Thruster", *39th AIAA/ASEE/ASME Joint Propulsion Conference, Huntsville, Alabama*. American Institute of Aeronautics and Astronautics, Washington, DC, 2003. AIAA-2003-5154

[8]Bareilles J., Hagelaar G. J. M., Garrigues L., Boniface C., Boeuf J. P. and Gascon N., "Critical Assessment of a Two-Dimensional Hybrid Hall Thruster Model: Comparisons with Experiments", *Physics of Plasmas* Vol. 11, No 6, pp. 3035-3046, 2004.

[9]Barral, S., Makowski, K., Peradzynski, Z., Gascon, N., and Dudeck, M., "Wall Material Effects in Stationary Plasma Thrusters II: Near-Wall and Inner-Wall Conductivity," *Physics of Plasmas*, Vol. 10, No. 10, Oct. 2003, p. 4137.